Reactions of Ta^+ and W^+ with H_2, D_2, and HD: Effect of lanthanide contraction and spin–orbit interactions on reactivity and thermochemistry

Xiao-Guang Zhang, Chad Rue, Sae-Young Shin, and P. B. Armentrout
Department of Chemistry, University of Utah, Salt Lake City, Utah 84112-0850

(Received 16 November 2001; accepted 9 January 2002)

A guided ion beam tandem mass spectrometer is used to examine the kinetic energy dependence of reactions of the third-row transition metal cations, Ta^+, and W^+, with molecular hydrogen and its isotopologs. A flow tube ion source produces Ta^+ and W^+ ions in their electronic ground state term and primarily in the lowest spin–orbit level. Corresponding state-specific reaction cross sections are obtained. Modeling of the endothermic reaction cross sections yields the 0 K bond dissociation energies in eV (kJ/mol) of $D_0(Ta^+-H)=2.38\pm0.06$ (230 ± 6) and $D_0(W^+-H)=2.27\pm0.05$ (219 ± 5). The experimental thermochemistry is consistent with *ab initio* calculations, performed here and from the literature, which also provide the electronic structures of these species and details about the reaction surfaces. Results from reactions with HD provide insight into the reaction mechanisms and indicate that these early metal ions, Ta^+ and W^+, react largely via insertion mechanisms. Results for these third-row transition metal systems are compared with the first-row and second-row congeners and found to have higher reactivity towards dihydrogen and stronger M^+-H bonds. These differences can be attributed to the lanthanide contraction, relativistic effects, and efficient spin–orbit interactions among surfaces of different spin. © *2002 American Institute of Physics.* [DOI: 10.1063/1.1456029]

I. INTRODUCTION

In the preceding paper,[1] we reviewed previous studies of the reactions of atomic metal ions with dihydrogen, reaction (1), and its isotopic analogs, reactions (2)–(4),

$$M^+ + H_2 \rightarrow MH^+ + H, \quad (1)$$

$$M^+ + D_2 \rightarrow MD^+ + D, \quad (2)$$

$$M^+ + HD \rightarrow MH^+ + D, \quad (3)$$

$$M^+ + HD \rightarrow MD^+ + H. \quad (4)$$

We also examined the utility of detailed studies of such a simple reaction and pointed out that they are of obvious fundamental interest, have implications for understanding a variety of catalytic reactions involving transition metal systems, and form an ideal interface between experiment and theory. Among the third-row transition metal cations, only La^+ and Lu^+ had been previously studied.[2] The preceding paper added Pt^+ to this list and in this work, we report absolute cross sections as a function of kinetic energy for reactions of dihydrogen with Ta^+ and W^+. These data are analyzed to acquire $D_0(M^+-H)$. Electronic structures and potential energy surfaces for reaction are explored using theoretical calculations on the MH^+ and MH_2^+ species. Further, reactions (3) and (4) provide additional details regarding the reaction mechanisms, as has been shown previously.[3,4] Finally, we compare the reactivities and mechanisms of these two transition metal ions with those of their congeners in the first and second transition metal series.[5–7]

II. EXPERIMENT AND THEORY

A. General experimental procedures

The guided ion beam tandem mass spectrometer on which these experiments were performed has been described in detail previously.[8,9] The procedures used here directly follow those detailed in the preceding work,[1] so only differences associated with the use of W^+ and Ta^+ are outlined here. These differences are associated with the source, which again involves our direct current discharge flow tube (DC/FT) source.[9] In this work, the cathode is either a tantalum or tungsten rod, which are sputtered by Ar^+ ions created in the discharge. The ions undergo $\sim10^5$ thermalizing collisions with He and $\sim10^4$ collisions with Ar before entering the guided ion beam apparatus, which appears to be adequate to form Ta^+ ions in their ground electronic state. To ensure that any excited states of W^+ are quenched, small amounts of methane are added to the flow gases about 40 cm downstream of the source.[10] Methane pressures are kept low to minimize reactions that produce WCH_2^+, therefore decreasing the desired ion intensity.

With the addition of such cooling gases, the DC/FT source produces metal ions in the ground state. As outlined in the preceding paper,[1] previous work indicates that ions should have effective temperatures conservatively estimated as about 700 ± 400 K (Table I). Therefore, the ions are believed to be in the ground electronic state term, $a\,^5F(6s^15d^3)$ for Ta^+ and $a\,^6D(6s^15d^4)$ for W^+, and largely in the lowest spin–orbit level. From the populations of ions at 700 ± 400 K, the average electronic energies are calculated to be $0.025+0.038/-0.024$ eV for Ta^+ and $0.017+0.040/-0.017$ eV for W^+. These estimated popula-

TABLE I. Electronic states of third row transition metal cations.[a]

Ion	State	J	Electron configuration	Energy (eV)	Population (%)[b] 300 K	700 K	1100 K
Ta^+	$a\,^5F$	1	$6s^15d^3$	0.000	98.83	82.43	64.67
		2		0.128	1.17	16.49	27.97
		3		0.328	0.0	0.84	4.76
		4		0.547	0.0	0.03	0.60
		5		0.767	0.0	0.0	0.07
	$a\,^3F$	2	$6s^25d^2$	0.394	0.0	0.20	1.68
		3		0.847	0.0	0.0	0.02
		4		1.208	0.0	0.0	0.0
	$a\,^3P$	0	$6s^25d^2$	0.511	0.0	0.01	0.10
		1		0.661	0.0	0.0	0.06
		2		0.702	0.0	0.0	0.07
W^+	$a\,^6D$	1/2	$6s^15d^4$	0.000	99.86	91.50	75.09
		3/2		0.188	0.14	8.07	20.60
		5/2		0.393	0.0	0.40	3.55
		7/2		0.585	0.0	0.02	0.63
		9/2		0.762	0.0	0.0	0.12
	$a\,^6S$	3/2	$5d^5$	0.920	0.0	0.0	0.01
	$a\,^4P$	avg	$6s^15d^4$	1.453	0.0	0.0	0.0
	$a\,^4F$	avg	$6s^15d^4$	1.587	0.0	0.0	0.0

[a]Reference 18.
[b]Maxwell–Boltzmann distribution at the indicated temperature.

TABLE II. Calculated vibrational frequencies and zero point energies for H_2, MH^+, and MH_2^+.[a]

Species	Frequency (cm^{-1})	Zero point energy (eV)
H_2	4331	0.268
Ta^+–H($^4\Sigma^-$)	1908	0.118
($^4\Phi$)	1907	0.118
($^4\Pi$)	1770	0.110
TaH_2^+($^3B_1$)	676, 1946, 1950	0.283
($^3A_1$)	648, 1954, 1958	0.283
($^3A_2$)	545, 1919, 1956	0.274
($^3B_2$)	609, 1890, 1921	0.274
($^5B_1$)	427, 1097, 1488	0.187
($^5A_1$)	425, 1096, 1492	0.187
($^5A_2$)	346, 931, 1465	0.170
W^+–H($^5\Pi$)	1986	0.123
($^5\Delta$)	2006	0.124
($^5\Sigma^+$)	1926	0.119
WH_2^+($^6A_1$)[b]	984, 1315, 3450	0.356
($^4B_1$)	538, 1366, 2041	0.245
($^4B_2$)	436, 2018, 2035	0.278
($^4A_2$)	524, 2045, 2457	0.312
($^4A_1$)	708, 1813, 1951	0.277

[a]Calculations using B3LYP/6−311+G(3p) on H and the Hay–Wadt relativistic ECP (Ref. 15) as adjusted for the metal cation by Ohanessian *et al.* (Ref. 16). Values have been scaled by 0.9804 (Ref. 17).
[b]This species has an M^+–(H_2) structure, whereas all others have H–M^+–H structures.

tions are consistent with the failure to observe any evidence for electronically excited M^+ species in the present and related studies,[10] once the cooling gases are added to the flow tube.

Analysis of the cross section data is performed as outlined in the preceding paper,[1] and again involves the use of Eq. (5) to reproduce the kinetic energy dependence of the cross sections,

$$\sigma(E)=\sigma_0\sum g_i(E+E_{\mathrm{el}}+E_i-E_0)^n/E. \quad (5)$$

Here σ_0 is an energy-independent scaling factor, E is the relative kinetic energy of the reactants, E_{el} is the electronic energy of the metal cation, and n is an adjustable parameter. The sum considers contributions from rovibrational states of the neutral reactants at 300 K, denoted by i, having energies E_i and populations g_i, where $\Sigma g_i=1$. In this analysis, the average electronic energies are chosen as 0.03 ± 0.03 eV for both metal ions, as noted above. These uncertainties are included in the final thermochemistry reported.

B. Theoretical calculations

All quantum chemistry calculations reported here are computed using the B3LYP hybrid density functional method,[11,12] and performed with the GAUSSIAN 98 suite of programs.[13] A large basis set is used for hydrogen, triple zeta with diffuse and polarization functions, 6-311+G(3p). This basis set gives good results for the thermochemistry of dihydrogen, with deviations from experiment of less than 0.03 eV for the bond energy of H–H (4.505 eV calculated versus 4.478 eV experimental[14]). The 60 core electrons of tantalum and tungsten are described by the relativistic effective core potentials (ECPs) of Hay–Wadt (HW),[15] equivalent to the Los Alamos double zeta ECP (LANL2DZ) basis set. The HW-ECP is optimized for neutral atoms, whereas the positive charge differentially contracts the s orbitals compared to the d orbitals. Hence, all calculations were performed with an altered HW-ECP basis for Ta and W as described by Ohanessian *et al.* (HW+).[16] In all cases, the thermochemistry calculated here is corrected for zero point energies, which were explicitly calculated for each state of H_2, TaH^+, WH^+, TaH_2^+, and WH_2^+. The calculated frequencies, scaled by 0.9804,[17] are listed in Table II.

In all cases, the experimental BDEs refer to the ground spin-orbit state at 0.0 eV: $a\,^5F_1$ for Ta^+ and $a\,^6D_{1/2}$ for W^+.[18] In contrast, calculations are referenced to the properly weighted mean of all spin–orbit levels in the ground state term: 0.466 eV for $Ta^+(a\,^5F)$ and 0.514 eV for $W^+(a\,^6D)$.[18] Because our calculations do not explicitly include spin–orbit interactions, all calculated bond energies must be corrected for these different asymptotic energies to properly compare with experimental values. This correction improves the agreement between experiment and the theory conducted here, a result also obtained in the preceding paper[1] and in our work on $PtCH_x^+$ species.[19] Likewise the description of the generalized valence bond (GVB) calculations of Ohanessian *et al.*[16] and the calculations of Balasubramanian and co-workers[20,21] suggest that such corrections may also need to be applied to their reported bond energies in order to properly compare with our experimental results. (Although it is also possible that such corrections have already been made.) As will be seen below, however, the literature values as reported generally agree better with our present experimental and theoretical values. Consequently, we do not apply such a correction to their values in the results and discussion below.

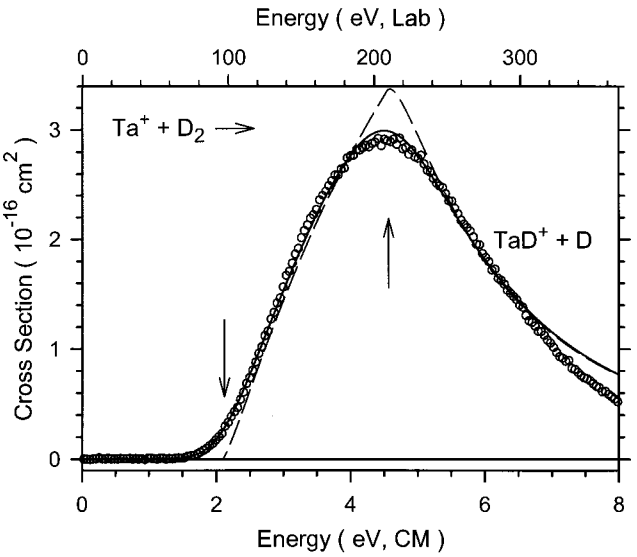

FIG. 1. Cross sections for reaction of Ta^+ ($a\,^5F$) with D_2 as a function of kinetic energy in the center-of-mass frame (lower axis) and laboratory frame (upper axis). The best fit of Eq. (5) with parameters of Table III to the data is shown as a dashed line. The solid line shows this model convoluted over the kinetic and internal energy distributions of the reactant neutral and ion. Arrows indicate E_0 and D_0(D–D) at 4.56 eV.

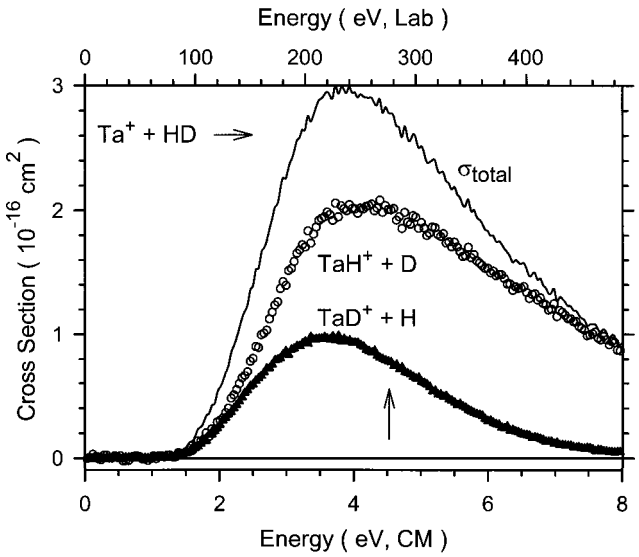

FIG. 3. Cross sections for reaction of Ta^+ ($a\,^5F$) with HD as a function of kinetic energy in the center-of-mass frame (lower axis) and laboratory frame (upper axis). The arrow indicates D_0(H–D) at 4.51 eV.

III. EXPERIMENTAL RESULTS

A. Reactions with D_2 and H_2

Figures 1 and 2 show cross sections as a function of kinetic energy for the bimolecular reaction of D_2 with Ta^+ and W^+ produced in the DC/FT source. A single product ion, as shown in reaction (2), is observed in all cases. Similar reactions with H_2 were also performed and yield consistent results. The magnitudes of the $M^+ + H_2$ reaction cross sections either match those for the $M^+ + D_2$ reactions or differ within the 20% experimental uncertainty of these absolute cross section measurements when the same mass resolution for the quadrupole mass spectrometer is used for these two metal systems. Only results of the reaction $M^+ + D_2$ are presented here because the heavier isotope reduces mass overlap between the product ion and the much more intensive primary ion, thereby allowing intensities of the product ion to be measured more accurately over a larger dynamic range.

Both systems exhibit cross sections that rise from an apparent threshold that is similar in both systems. They both reach maxima with comparable magnitudes near the dissociation energy of D_2, 4.56 eV.[14] Above this energy, MD^+ may be formed with an internal energy in excess of its bond dissociation energy. Thus, the MD^+ product begins to dissociate in the overall reaction (6),

$$M^+ + D_2 \rightarrow MD^+ + D \rightarrow M^+ + D + D. \tag{6}$$

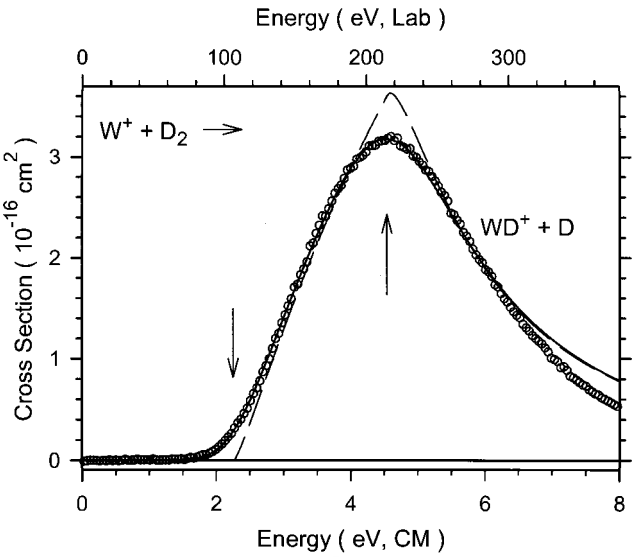

FIG. 2. Cross sections for reaction of W^+ ($a\,^6D$) with D_2 as a function of kinetic energy in the center-of-mass frame (lower axis) and laboratory frame (upper axis). The best fit of Eq. (5) with parameters of Table III to the data is shown as a dashed line. The solid line shows this model convoluted over the kinetic and internal energy distributions of the reactant neutral and ion. Arrows indicate E_0 and D_0(D–D) at 4.56 eV.

B. Reactions with HD

In the reactions of M^+ with HD, both reactions (3) and (4) are observed, as shown in Figs. 3 and 4 for $M^+ = Ta^+$ and W^+, respectively. Because of the close proximity of the product masses, there is some overlap between these signals at the mass resolution used in the quadrupole mass filter. Resolution could not be increased further without sacrificing efficient collection of the product ions. This mass overlap has been carefully measured by determining peak shapes with and without gas in the collision cell. Although the similar energy dependence of the two products makes such measurements somewhat difficult, the mass overlap contribution of the higher mass MD^+ channel to the MH^+ channel has been subtracted in the cross sections shown. The accuracy of this correction is confirmed by good agreement between the magnitudes of the total cross sections for the HD systems and those of the H_2 and D_2 systems (Figs. 1–4).

In both metal systems, both MH^+ and MD^+ cross sections exhibit endothermic behavior and rise from thresholds

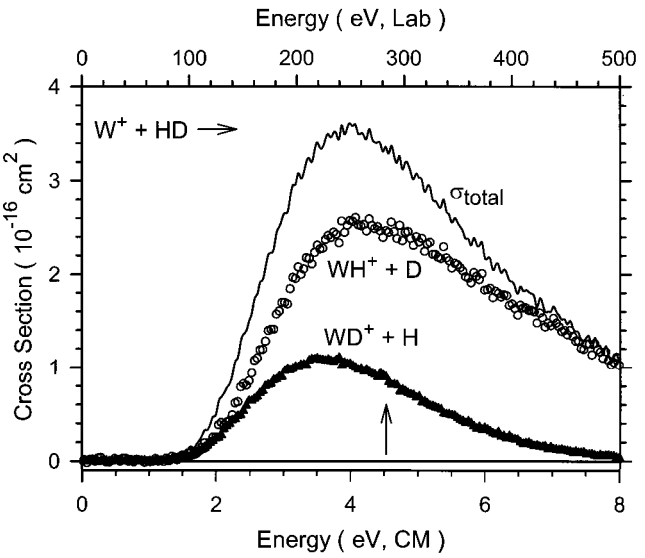

FIG. 4. Cross sections for reaction of W^+ ($a\,^6D$) with HD as a function of kinetic energy in the center-of-mass frame (lower axis) and laboratory frame (upper axis). The arrow indicates D_0(H–D) at 4.51 eV.

that are similar to each other and to those of the H_2 and D_2 systems. The cross sections of MH^+ and MD^+ peak slightly below the bond dissociation energy of HD, 4.51 eV,[14] with those for MD^+ peaking at somewhat lower energies than those of MH^+. The total cross sections in the HD systems are similar in shape to the D_2 and H_2 data at energies below the maximum cross section, whereas at higher energies, the total cross sections, largely attributable to the $MH^+ + D$ channels, exceed those of the D_2 and H_2 systems. The high-energy behavior indicates that the D atom carries away more energy from MH^+ than the H atom carries away from MD^+, and more than the neutral product carries away in the H_2 and D_2 systems, as well. This interesting effect is typical of atomic metal ion reactions with H_2, HD, and D_2,[1,4,7,22] and has been discussed in detail elsewhere.[4,5,23,24]

IV. THERMOCHEMICAL AND THEORETICAL RESULTS

A. Experimental bond energies

The endothermic cross sections in each reaction system are analyzed in detail using Eq. (5). Typical models are shown in Figs. 1 and 2 and can be seen to reproduce the experimental results very well. At energies above the onset of reaction (6), our analyses include a model for this subsequent dissociation, as outlined in detail elsewhere.[25] This model relies on two parameters, E_D, the onset for MH^+ (MD^+) dissociation in reaction (6), and p, a parameter similar to n in Eq. (5). For the results shown in Figs. 1 and 2, E_D is fixed to the H_2 (D_2) bond energy and the optimum value of p was found to be 2.0.

The optimum values of the parameters in Eq. (5) are listed for these systems in Table III. These values represent the average of between 3–5 data sets for each system. Note that the thresholds listed differ appreciably from the apparent thresholds for these reactions as shown in Figs. 1 and 2. This is largely because of the appreciable kinetic energy distribution of the light D_2 reactant. Because the rotational, vibrational, translational, and electronic energy distributions of reactants are explicitly included in the modeling, the E_0 threshold energies determined using Eq. (5) correspond to 0 K values. From the thresholds measured, the BDEs for the metal–ligand cations observed in reactions (1) and (2) can be calculated using Eq. (7),

$$D_0(M^+–L) = D_0(L–L) - E_0, \tag{7}$$

where D_0(H–H) = 4.478 eV and D_0(D–D) = 4.556 eV.[14] This equation assumes that there is no activation barrier in excess of the endothermicity of the reaction, an assumption that is often true for ion–molecule reactions because of the long-range attractive forces.[26]

TABLE III. Parameters of Eq. (5) used in modeling reactions (1) and (2) and the bond energies derived.

Reaction	σ_0	n	E_0 (eV)	$D_0(M^+–H)$ (eV)
$Ta^+ + D_2$	5.1±0.3	1.2±0.1	2.16±0.06	2.37±0.06[a]
$Ta^+ + H_2$	4.7±0.4	1.2±0.1	2.09±0.08	2.39±0.08
$W^+ + D_2$	5.8±0.3	1.3±0.1	2.24±0.06	2.28±0.06[a]
$W^+ + H_2$	6.5±0.4	1.2±0.1	2.23±0.06	2.25±0.06

[a]Values corrected for zero-point energy differences. See text.

Table III provides a summary of the $M^+–H$ bond energies derived from the present experiments with both H_2 and D_2. For the D_2 results, this requires correcting for the zero point energy differences between MD^+ and MH^+, which was accomplished using vibrational frequencies of 2006 cm^{-1} for TaH^+ and 2065 cm^{-1} for WH^+.[16] The vibrational frequencies of MD^+ are calculated from those of MH^+ according to $\omega_{MD} = \omega_{MH}(\mu_{MH}/\mu_{MD})^{1/2}$. Thus the zero point energy differences in the MH^+ and MD^+ bond energies are 0.036 and 0.037±0.004 eV for M = Ta and W, respectively, assuming 10% uncertainties in the frequencies. [Use of the 1908 or 1986 cm^{-1} frequencies calculated here for $TaH^+(^4\Sigma^-)$ or $WH^+(^5\Pi)$, Table II, yields differences of 0.034 and 0.036 eV, respectively, which do not change the final results.] Note that the $M^+–H$ bond energies obtained from the H_2 and D_2 systems are in excellent agreement with one another (Table III). We take the average of these two values as our final experimental determinations: 2.38 ±0.06 eV for $Ta^+–H$ and 2.27±0.05 eV for $W^+–H$.

B. $Ta^+–H$

Generalized valence bond (GVB) calculations indicate that the $Ta^+–H$ bond in the $^4\Sigma^-$ state is formed by covalent interaction between a singly occupied sd hybridized orbital on Ta^+ (60% $5d$ and 39% $6s$) and the singly occupied $1s$ orbital on H.[16] Such hybridization is particularly efficient in the third-row transition metals because lanthanide contraction and relativistic effects make the $6s$ orbital comparable in size and energy to the $5d$ orbitals. The calculations also indicate that there is a low-lying $^4\Phi$ state, calculated to lie only 0.04 eV above the $^4\Sigma^-$ state.[16] The $^4\Sigma^-$ and $^4\Phi$ states differ primarily in their occupied $5d$ nonbonding orbitals, $\sigma\pi^2$ (mixed with $\sigma\delta^2$) and $\sigma\pi\delta$, respectively. Both states can be formed from interaction of ground state $Ta^+(a\,^5F, 6s^1 5d^3)$ with $H(^2S, 1s)$, such that no promotion to

TABLE IV. Experimental and theoretical bond energies (in eV) for MH_x^+ ($x=1$ and 2).

Species	Experiment	Theory[a] This work	Theory[a] Literature[b]
$Ta^+-H(^4\Sigma^-)$	2.38 ± 0.06	2.09	2.34[c]
$(^4\Phi)$		2.21	2.30[c]
$(^4\Pi)$		1.57	2.08[c]
$Ta^+-H_2(^3B_1)$		0.57	0.78 (0.18)[d]
$(^3A_1)$		0.42	0.65 (0.07)[d]
$(^3A_2)$		0.42	0.56 (0.00)[d]
$(^3B_2)$		0.22	0.35 (−0.25)[d]
$(^5B_1)$		−1.85	−1.86 (−2.35)[d]
$(^5A_1)$		−1.79	−1.91 (−2.37)[d]
$(^5A_2)$		−1.99	
$W^+-H(^5\Pi)$	2.27 ± 0.05	2.11_8	2.16[c]
$(^5\Delta)$		2.12_4	2.09[c]
$(^5\Sigma^+)$		1.95	1.96[c]
$W^+-H_2(^6A_1)$[e]		0.27	0.72 (0.42)[f]
$(^4B_1)$		0.30	0.24 (−0.37)[f]
$(^4B_2)$		0.25	0.16 (−0.40)[f]
$(^4A_2)$		0.22	0.19 (−0.42)[f]
$(^4A_1)$		−2.35	−2.79 (−2.03)[f]

[a]Calculations using B3LYP/6-311+G(3*p*) on H and Hay–Wadt relativistic ECP (Ref. 15) as adjusted for metal cations by Ohanessian *et al.* (Ref. 16). All values corrected for zero point energies and for the experimental spin–orbit state asymptote of M^+.
[b]Values may need to be corrected for the spin–orbit splitting of the M^+ asymptote. See text.
[c]Ohanessian *et al.* (Ref. 16).
[d]Dai, Cheng, and Balasubramanian (Ref. 20). MRSDCI (CASSCF) values.
[e]This species has an $M^+-(H_2)$ structure, whereas all others have $H-M^+-H$ structures.
[f]Balasubramanian and Ma (Ref. 21). MRSDCI (CASSCF) values.

TABLE V. Theoretical geometries for MH_x^+ ($x=1$ and 2).

Species	This work[a] r_e (M–H, Å)	This work[a] ∠HMH (°)	Literature r_e (M–H, Å)	Literature ∠HMH (°)
$Ta^+-H(^4\Sigma^-)$	1.742		1.741[b]	
$(^4\Phi)$	1.727		1.727[b]	
$(^4\Pi)$	1.761		1.740[b]	
$TaH_2^+(^3B_1)$	1.726	108.4	1.732[c]	110.3
$(^3A_1)$	1.722	110.9	1.731[c]	115.8
$(^3A_2)$	1.720	84.3	1.723[c]	87.0
$(^3B_2)$	1.734	98.2	1.740[c]	100.2
$(^5B_1)$	1.857	153.6	1.865[c]	148.8
$(^5A_1)$	1.857	153.8	1.873[c]	155.9
$(^5A_2)$	1.892	153.2		
$W^+-H(^5\Pi)$	1.692		1.701[b]	
$(^5\Delta)$	1.671		1.678[b]	
$(^5\Sigma^+)$	1.702		1.707[b]	
$WH_2^+(^6A_1)$[d]	1.928	24.0	1.961[e]	23.2
$(^4B_1)$	1.679	104.2	1.690[e]	106.2
$(^4B_2)$	1.681	94.8	1.685[e]	104.9
$(^4A_2)$	1.674	103.2	1.680[e]	100.7
$(^4A_1)$	1.741	139.4	1.856[e]	180.0

[a]Calculations using B3LYP/6−311+G(3*p*) on H and the Hay–Wadt relativistic ECP (Ref. 15) as adjusted for the metal cation by Ohanessian *et al.* (Ref. 16).
[b]Ohanessian *et al.* (Ref. 16).
[c]Dai, Cheng, and Balasubramanian (Ref. 20). MRSDCI values.
[d]This species has an $M^+-(H_2)$ structure, whereas all others have $H-M^+-H$ structures.
[e]Balasubramanian and Ma (Ref. 21). MRSDCI values.

an excited electronic state is required. These authors suggest that the $^4\Phi$ state could be the ground state once spin–orbit coupling corrections are considered.[16] Our B3LYP calculations using the HW+ECP find a $^4\Phi$ ground state, with the $^4\Sigma^-$ state lying another 0.12 eV higher, Table IV. Overall, it seems likely that the $^4\Phi$ state is the true ground state for TaH^+.

The average of the Ta^+-H bond energies determined from the H_2 and D_2 systems (Table III) is 2.38 ± 0.06 eV. This is in good agreement with the theoretical value of 2.34 eV (Table IV) calculated for the $^4\Sigma^-$ state using GVB theory followed by correlation consistent configuration interaction (CCCI) calculations.[16] [Note that this agreement suffers considerably if the theoretical value is lowered by 0.466 eV, the mean spin–orbit energy of the $Ta^+(a\,^5F)$ state, as discussed above.] Our B3LYP calculations (which includes a correction for the proper spin–orbit asymptote) also provide reasonable agreement, obtaining a bond energy of 2.21 eV (Table IV) for the $^4\Phi$ state. (Note that the agreement with experiment is worse in this case if the correction for the spin–orbit asymptote is not made.) Comparison of the calculated bond lengths for the low-lying states is also reasonable as shown in Table V.

C. W^+-H

GVB calculations indicate that the W^+-H bond in the $^5\Pi$ ground state is formed by covalent interaction between a singly occupied *sd* hybridized orbital on W^+ (59% 5*d* and 40% 6*s*) and the singly occupied 1*s* orbital on H.[16] The calculations also indicate that there is a low-lying $^5\Delta$ state, which is calculated to lie only 0.07 eV above the $^5\Pi$ state.[16] Spin–orbit coupling could alter the ordering of these states. Our calculations using the HW+ECP find that the $^5\Delta$ state is the ground state, but only lies 0.006 eV lower than the $^5\Pi$ state. Clearly, the true ground state for WH^+ cannot be unambiguously assigned. Both calculations also find an excited $^5\Sigma^+$ state having a bond energy of about 1.95 eV (Table IV). The $^5\Pi$, $^5\Delta$, and $^5\Sigma^+$ states differ primarily in their occupied 5*d* nonbonding orbitals, $\sigma\pi\delta^2$, $\sigma\pi^2\delta$, and $\pi^2\delta^2$, respectively. All three states can be formed from interaction of ground state $W^+(a\,^6D,6s^15d^4)$ with $H(^2S,1s)$, such that no promotion to an excited electronic state is required.

The average of the W^+-H bond energies determined from the H_2 and D_2 systems (Table III) is 2.27 ± 0.05 eV. This is slightly larger than the theoretical value of 2.16 eV (Table IV) calculated using GVB/CCCI theory.[16] The calculations performed here (including a correction for the proper spin–orbit asymptote) provide a comparable value of 2.12 eV (Table IV). Comparison of the calculated bond lengths for the low-lying states is also reasonable as shown in Table V.

D. $H-M^+-H$

To explore coarse features of the potential energy surface for reactions (1), we also calculated the properties of stable MH_2^+ complexes. Our results can be compared directly with those of Balasubramanian and co-workers, who calculated

the potential energy surfaces (PESs) for interaction of several states of the metal ions with H_2 in C_{2v} symmetry at the complete active space self-consistent field (CASSCF) level.[20,21] These calculations use a relativistic effective core potential on Ta and W that retains the ns, $(n-1)s$, $(n-1)p$, and $(n-1)d$ orbitals in the valence space. Single point calculations on the stationary points were then conducted at a multireference single and double configuration interaction (MRSDCI) level.

For TaH_2^+, we calculate a Ta^+-H_2 BDE of 0.57 eV for the $^3B_1$ ground state, comparable to the MRSDCI value, 0.78 eV, of Dai, Cheng, and Balasubramanian (DCB).[20] [It is possible that the latter value exceeds our value because the value of DCB has not been corrected for the mean spin-orbit energy of the $Ta^+(a\,^5F)$ state, 0.466 eV as discussed above.] Our calculations for other low-lying triplet states of TaH_2^+ (Table IV) find comparable relative energies as those determined by DCB. Our calculations also find that the quintet states of TaH_2^+ are well above the $Ta^+(a\,^5F)+H_2$ asymptote, again in good agreement with the previous work.[20] Geometries of all states calculated here agree with the MRSDCI structures of DCB generally within 0.01 Å for bond lengths and within 5° for bond angles with our results being systematically smaller (Table V).

For WH_2^+, our bond energies for the quartet states are comparable to the MRSDCI calculations of Balasubramanian and Ma (BM), Table IV.[21] These authors find that the ground state for WH_2^+ is $^6A_1$, which corresponds to an H_2 adduct, i.e., the H–W–H bond angle is small, indicating that the H_2 bond length is largely unperturbed. We also find this state but our calculations find that it is bound less strongly by 0.45 eV, a result that may be because our value has been corrected for the mean spin–orbit energy of the $W^+(a\,^6D)$ state, 0.514 eV as discussed above. Our calculations indicate that this $^6A_1$ state has a comparable energy to the $^4B_1$ state (Table IV). Details of the calculated geometries for WH_2^+ are given in Table V, where it can be seen that there is good agreement between our work and that of BM.[21]

In our work on the PtH_2^+ potential energy surfaces,[1] we found systematic differences between the CASSCF surfaces calculated by Zhang and Balasubramanian[27] and the B3LYP surfaces calculated in our work. Hence, in the present study, we also performed B3LYP/HW+/6-311+G(3p) calculations for the C_{2v} surfaces of TaH_2^+ and WH_2^+. Our results are shown in Figs. 5 and 6, respectively. Starting with the less complicated tungsten system, Fig. 6, we find that the relative behavior of these surfaces is very similar to that of BM; however, our quartet surfaces are much more attractive at large angles. As noted above, our quartet surfaces reach minima that are bound with respect to the reactant asymptote, in agreement with the single point MRSDCI calculations of BM. BM also calculated several other sextet surfaces evolving from the $W^+(^6D)+H_2$ asymptote and a $^4A_1$ surface. These surfaces were found to be strongly repulsive at long range, hence, we did not pursue calculations on these surfaces.

Qualitatively similar results are obtained for the TaH_2^+ surfaces, Fig. 5. In agreement with DCB, the quintet surfaces evolving from the ground state $Ta^+(a\,^5F)+H_2$ asymptote

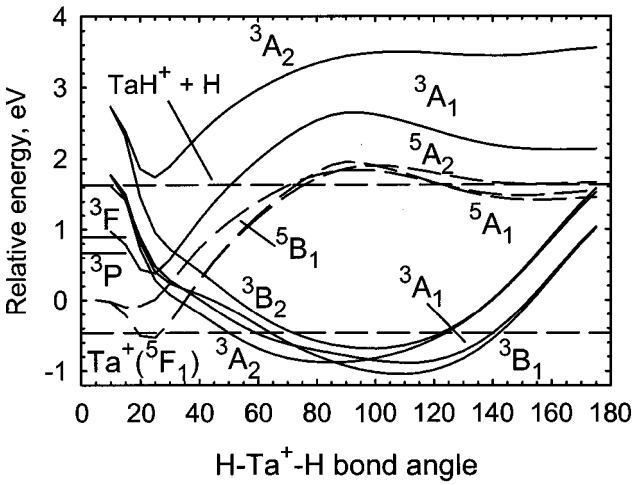

FIG. 5. B3LYP/HW+/6-311+G(3p) calculations of the potential energy surfaces for the interaction of Ta^+ with H_2 in C_{2v} symmetry as a function of the H–Ta^+–H bond angle in degrees. The experimental energy of the Ta^+ ($a\,^5F_1$) ground state at −0.466 eV is indicated as is the experimental energy of the TaH^+ + H products (2.10 eV above the experimental $a\,^5F_1$ ground state).

are largely repulsive, although we do find a long-range (small angle) minimum along the $^5A_1$ surface. The relative behavior of the triplet surfaces at large angles agrees nicely, as noted above, but again our surfaces are more strongly bound than the CASSCF surfaces, in reasonable agreement with the MRSDCI single point results. In addition, we find more attractive triplet surfaces at long range, in contrast to the results of DCB which exhibit repulsive behavior for all triplet surfaces, with the possible exception of the $^3A_2$, which is relatively flat. However, it is clear that the surfaces of DCB are adiabatic and show evidence of crossings from surfaces evolving from higher energy asymptotes. In contrast, our calculated surfaces are diabatic and only in the case of an excited $^3A_1$ surface does the asymptotic energy at small

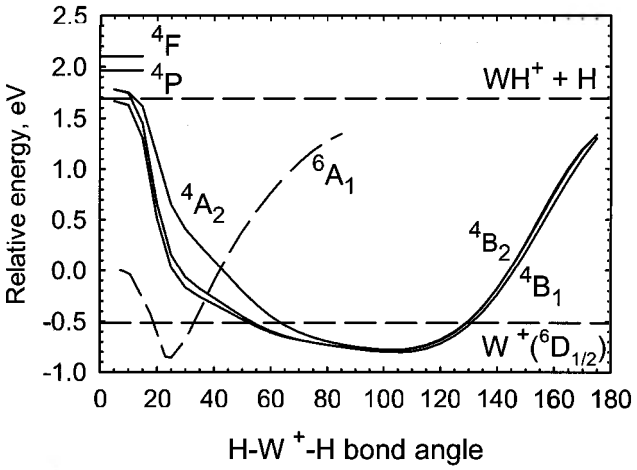

FIG. 6. B3LYP/HW+/6-311+G(3p) calculations of the potential energy surfaces for the interaction of W^+ with H_2 in C_{2v} symmetry as a function of the H–W^+–H bond angle in degrees. The experimental energy of the W^+ ($a\,^6D_{1/2}$) ground state at −0.514 eV is indicated as is the experimental energy of the WH^+ + H products (2.21 eV above the experimental $a\,^6D_{1/2}$ ground state).

angles approach that corresponding to the low-lying $Ta^+(a\,^3P)$ or $Ta^+(a\,^3F)$ states. Hence, the long-range (small angle) behavior shown in Fig. 5 is incomplete and can probably be best envisioned by imagining an avoided crossing between the two $^3A_1$ surfaces. Similar behavior is likely for the other low-lying triplet surfaces.

In all of the calculations of DCB, BM, and Figs. 5 and 6, the symmetry was restricted to C_{2v} and excited surfaces having the same symmetry as lower energy surfaces were not included, except for $^3A_1$ and $^3A_2$ surfaces of TaH_2^+ performed here. Because of the symmetry restriction, these PESs examine the evolution of $M^+ + H_2$ to the MH_2^+ species as a function of the H–M–H angle but cannot proceed onto the $MH^+ + H$ dissociation asymptote. Although Balasubramanian and coworkers did not calculate PESs for the production of $MH^+ + H$, these products are almost certainly formed from the MH_2^+ intermediates with no additional barriers. Ground states of $TaH^+(^4\Phi, ^4\Sigma^-)$ and $WH^+(^5\Delta, ^5\Pi)$ interact with $H(^2S)$ to form both low-spin and high-spin states of MH_2^+. Formation of low-spin states involves covalent coupling of a nonbonding MH^+ electron with H, such that the PESs should be strongly attractive. Formation of high-spin states involves donation of the electron on H into an empty orbital on MH^+ and this should also lead to modestly attractive surfaces. Therefore, we do not anticipate any barriers in the exit channels of reaction (1) and its isotopologs for either metal system. To verify this, we performed relaxed potential energy surface scans at the B3LYP level starting with the ground state MH_2^+ species and systematically lengthening one of the M–H bonds. These scans follow a $^3A''$ surface for TaH_2^+ (evolving from the $^3B_1$ ground state) and a $^4A'$ surface for WH_2^+ (evolving from the $^4B_2$ state). These surfaces lead directly to ground state $TaH^+(^4\Phi) + H$ and $WH^+(^5\Pi) + H$ products, respectively, with no barriers in excess of the endothermicity for both metal systems.

V. DISCUSSION

A. Intrinsic M^+–H bond dissociation energies

Periodic variations in the BDEs for the first-row transition metal hydride cations have been understood previously by means of promotion energy (E_p) arguments.[22,28–30] We define E_p as the energy associated with promoting the ground state of M^+ to a state having a suitable electronic configuration to form a covalent M^+–H bond, plus the spin-exchange energy associated with spin decoupling the bonding electron from the other electrons on the metal. This promotion energy is denoted as $E_p(s^1d^{x-1})$ if the bonding orbital on the metal is an s orbital or $E_p(d^x)$ if the bonding orbital is $d\sigma$, where x represents the total number of valence electrons. For the first-row transition metals, M^+–H BDEs exhibit an excellent correlation with $E_p(4s^13d^{x-1})$, implying that the dominant bonding character is $M^+(4s)$–$H(1s)$.[22,28] At a promotion energy of zero, the intrinsic $M^+(4s)$–$H(1s)$ bond energy is about 2.42 eV.[22,28] For the second-row transition metal systems, correlations with the promotion energy differ somewhat from the first-row transition metal systems. For the early metal ions, Y^+, Zr^+, Nb^+, and Mo^+,[7] the correlation of M^+–H BDEs with $E_p(5s^14d^{x-1})$ is reasonable, whereas the correlation with $E_p(4d^x)$ is satisfying for the late metal ions, Ru^+, Rh^+, Pd^+, and Ag^+.[31] As Y^+ has a very small promotion energy, the Y^+–H BDE represents a reasonable estimate for the "intrinsic" bond energy of $M^+(5s)$–$H(1s)$, 2.65 ± 0.08 eV.[7] This can be compared to the average value of 2.11 ± 0.12 eV found for a $M^+(4d\sigma)$–$H(1s)$ bond of the late second-row transition metals.[7] Overall, this behavior indicates that d orbital character in the M^+–H bonding increases significantly from the first-row to the second-row metals and increases as one moves across the second-row to Ru^+–H, Rh^+–H, and Pd^+–H,[7,31] consistent with theoretical calculations.[32,33]

For the third-row transition metals, there are still too few experimental data points to definitively explore correlations of M^+–H BDEs with promotion energies or to assign intrinsic bond energies. However, the promotion energy concept may be useful in understanding the relative BDEs. For the early third-row transition metal ions, we determine the $E_p(6s^15d^{x-1})$ promotion energies as the average excitation energy[18] for the low-spin and high-spin coupled states having a $6s^15d^{x-1}$ configuration. These promotion energies are 0.26 eV for La^+,[2] 1.17 eV for Ta^+, and 1.17 eV for W^+, whereas the BDEs are 2.48 eV for La^+–H, 2.38 eV for Ta^+–H, and 2.27 eV for W^+–H. Thus, there is no strong correlation between the promotion energies and the BDEs of these three metal ions, although the similar BDEs of TaH^+ and WH^+ are consistent with similar E_p values. Further, this result is consistent with GVB calculations, which find that the BDE+E_p values systematically increase across the Periodic Table.[16]

B. Reaction mechanisms and the effects of electronic configuration on reactivities

There are two main factors that influence the reactivity of the metal ion–dihydrogen reaction systems. One is the reaction thermochemistry, and the other is the electron configuration of M^+ and its spin state. In this study, the reactions of both metal ions with dihydrogen and its isotopologs are endothermic. Tantalum and tungsten cations exhibit similar reactivity (as measured by the cross section magnitudes) partially because they have similar thresholds (Table III). In contrast, the cross sections for reaction of platinum cations[1] are larger than those measured here, which is partly because this reaction has the smallest endothermicity among the three systems. To further understand these reactions, we need to consider the electron configuration of each metal ion and its effect on the reactivities and mechanisms. As noted in the preceding paper,[1] a fairly simple donor–acceptor model is useful in understanding σ-bond activation by atomic metal ions.

1. Tantalum reactions

The $a\,^5F$ ground state of Ta^+ ion has a high-spin $6s^15d^3$ electron configuration. According to the diabatic reactivity rules outlined in the preceding paper,[1] such an ion should react diabatically with dihydrogen according to "rule 3," i.e., via an impulsive mechanism. Such a prediction is inconsistent with the experimental cross sections (Fig. 3). However,

in agreement with this prediction, the calculated PESs for reaction of $Ta^+ + H_2$ indicate that the $Ta^+(a\,^5F)$ ground state has largely repulsive interactions with H_2 at long range (small H–Ta–H bond angles), Fig. 5.[20] As the bond angle increases, the energy rises until there are shallow minima along the quintet surfaces near angles of 180°, but the barriers to reach these minima exceed the energy of the $TaH^+ + H$ asymptote (and in the CASSCF calculations they are much higher). Therefore, the experimental behavior observed here at threshold is inconsistent with reaction along any of the quintet surfaces.

However, calculations indicate that there are several triplet surfaces evolving from $a\,^3P$ and $a\,^3F$ states of Ta^+, although as noted above, the triplet surfaces shown in Fig. 5 have not been correctly associated with the adiabatic asymptote. Both of these atomic triplet states have a $6s^25d^2$ configuration and hence are repulsive at long range (small angle) interactions with H_2, a result that is most evident in the CASSCF surfaces calculated by DCB.[20] As the angle increases, these surfaces evolve to form the various low-lying states of TaH_2^+ (Table IV) by mixing with surfaces evolving from higher-lying triplet states of Ta^+. This is clearly indicated by the PESs shown in Fig. 5. As noted above, these triplet states of TaH_2^+ are expected to dissociate to the ground state $TaH^+ + H$ without barriers in excess of the product asymptote once the energy available for the reaction is sufficiently high.

Therefore, reaction of $Ta^+ + H_2$ must occur at threshold by coupling the quintet and triplet surfaces, presumably involving the strong spin–orbit interactions of the third-row metals. The PESs calculated at the CASSCF level show that the quintet-triplet surfaces cross about 1.0 ± 0.2 eV above the $Ta^+(a\,^5F) + H_2$ asymptote. (It should be noted that the crossing points taken from such graphs correspond to the same angle for both states but may not have the same bond lengths for both states. Thus, the true crossing seam between these surfaces must occur at energies higher than those taken from such plots.) Our B3LYP calculations find that the crossing points lie between 0.0 and 0.6 eV relative to the $Ta^+(a\,^5F) + H_2$ asymptote, which puts them 0.4–1.0 eV above the experimental energy zero for $Ta^+(a\,^5F_1) + H_2$ reactants. This is still well below the threshold energy for product formation of 2.1 ± 0.06 eV measured for the $Ta^+ + H_2$ reaction (Table III). Therefore, the reaction occurs by crossing from one of several quintet surfaces to one of several triplet surfaces leading to inserted H–Ta^+–H intermediates, which are calculated to be more stable than reactants by about 0.8–0.2 eV (B3LYP and MRSDCI results, Table IV). The involvement of such stable intermediates is consistent with the observation of statistical behavior in the $Ta^+ + HD$ system at threshold (as indicated most clearly by a branching ratio close to unity, Fig. 7). At higher kinetic energies, it seems likely that the reaction can remain on the quintet surface with an increasing probability and still form products. Under these circumstances, the mechanism should become more direct, consistent with observation that the branching ratio increases to about 2.5 before the dissociation of the TaH^+/TaD^+ products can begin.

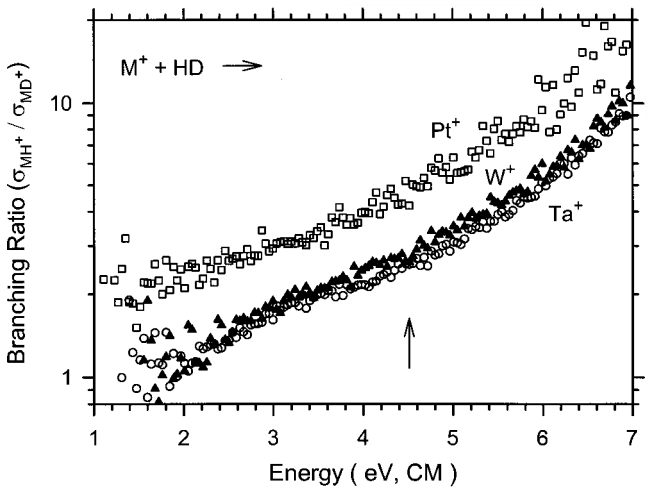

FIG. 7. Product branching ratios ($\sigma_{MH^+}/\sigma_{MD^+}$) for reactions of Ta^+ (open circles), W^+ (solid triangles), and Pt^+ (open squares) with HD as a function of kinetic energy in the center-of-mass frame. The arrow indicates D_0(H–D) at 4.51 eV.

2. Tungsten reactions

As for the high-spin state of Ta^+, the high-spin $a\,^6D(6s^15d^4)$ ground state of W^+ is not expected nor calculated to insert into H_2,[21] Fig. 6. Although a $W(H_2)^+$ adduct can be formed at long range (small H–W–H angle), the barrier for insertion into H_2 along the $^6A_1$ state (the lowest sextet surface) is calculated to lie higher than the $WH^+ + H$ dissociation asymptote.[21] The other sextet surfaces are even more repulsive than the $^6A_1$ surface. Therefore, the experimental behavior observed here at threshold is inconsistent with reaction along the sextet surfaces.

Quartet surfaces evolving from the $a\,^4P$ and $a\,^4F$ states of W^+ lead to bound quartet states of WH_2^+ having large H–W–H bond angles, Table V and Fig. 6. Because the $a\,^4P$ and $a\,^4F$ states have $6s^15d^4$ configurations with half-filled $6s$ orbitals, these low-spin surfaces are less repulsive than the low-spin surfaces in the tantalum system, which evolve from triplet states having $6s^25d^2$ configurations. Similar to the tantalum system, extensive coupling of the sextet surfaces to several quartet surfaces by strong spin–orbit interactions can provide an adiabatic reaction path. In the CASSCF calculations, the apparent surface crossings occur at about 1.1 ± 0.3 eV above the $W^+(a\,^6D) + H_2$ asymptote,[21] whereas the B3LYP calculations find them at -0.3 to 0.0 eV. The latter are 0.2–0.5 eV above the experimental zero of energy, $W^+(a\,^6D_{1/2}) + H_2$, well below the threshold of 2.23 ± 0.06 eV measured for the $W^+ + H_2$ reaction (Table III). This path forms the inserted H–W^+–H intermediate in one of several low-lying quartet states (Table IV and Fig. 6). The well depths of the inserted H–W^+–H intermediates with respect to the $WH^+ + H$ dissociation asymptote are about 2.5 eV (B3LYP or MRSDCI results, Table IV). As noted above, these quartet states of WH_2^+ can readily dissociate to the ground state of the $WH^+ + H$ products with no energy in excess of the endothermicity, once the energy available for the reaction is high enough.

Presuming the quartet inserted H–W^+–H intermediate is formed, it is reasonable that statistical behavior is ob-

served in the HD system, as seen from a branching ratio near unity at threshold in Fig. 7. Similar reactivity in the Ta^+ and W^+ systems is observed because the energies at which the low and high spin surfaces cross are fairly similar. At higher kinetic energies, it seems likely that the probability of remaining on the sextet surfaces increases, but now this pathway can form products. For this pathway, the mechanism should be more direct, consistent with the gradually increasing branching ratio with increasing energy, Fig. 7.

3. Collinear processes

As in the case of $Pt^+ + H_2$,[1] it is appropriate to ask whether the reactions of Ta^+ and W^+ might occur via collinear ($C_{\infty v}$) pathways rather than by the perpendicular (C_{2v}) paths discussed above. Indeed, reaction along the high-spin surfaces evolving from the $6s^15d^{x-1}$ ground states of the metal ions can be argued to be more favorable for a $C_{\infty v}$ approach than for a C_{2v} approach, in analogy with the $H+H_2$ reaction system. What differs for a collinear approach is the behavior of the low-spin surfaces. For W^+, surfaces evolving from the $a\,^6D(6s^15d^4)$, $a\,^4P(6s^15d^4)$, and $a\,^4F(6s^15d^4)$ states should essentially parallel one another at long-range, such that there will be little chance for interactions of the low-spin and high-spin surfaces. For Ta^+, surfaces evolving from the $a\,^5F(6s^15d^3)$ state will be less repulsive than those evolving from the $a\,^3P(6s^25d^2)$ and $a\,^3F(6s^25d^2)$ states, such that interactions between the low-spin and high-spin surfaces is unlikely. Overall, this makes collinear $C_{\infty v}$ reaction pathways much less favorable than the C_{2v} perpendicular pathways where interactions among the low and high-spin surfaces are apparently efficient. It is possible that such collinear pathways along the high-spin surfaces do contribute to the observed reactivity at higher energies, which could explain why the branching ratios increase to values more characteristic of direct processes, Fig. 7.

C. Comparison of reactivity with first-row and second-row transition metal systems

For group 5 metal cations, the ratio of reactivities with dihydrogen (as indicated by the maximum cross sections) is about 1:3:7.5 for V^+:Nb^+:Ta^+ and all three metal cations show evidence for an insertion mechanism in the reaction with HD.[5,7] These similarities hold even though V^+ and Nb^+ have the same valence electron configuration, $(n-1)d^4$, whereas the Ta^+ ground state has a $6s^15d^3$ electron configuration, which would be expected to react inefficiently with dihydrogen. As noted above, the enhanced reactivity for Ta^+ is apparently a result of efficient spin-orbit coupling between surfaces evolving from $Ta^+(a\,^5F)$ and low-spin triplet states of Ta^+. The reactivity for the tantalum system is also enhanced because it has a smaller endothermicity compared to the vanadium and niobium systems.[5,7] This strong Ta^+-H BDE results from efficient *sd* hybridization, which is a consequence of the lanthanide contraction and relativistic effects.[16]

For group 6 metal cations, the chromium system has about six times smaller reactivity towards dihydrogen than the molybdenum system. Even though these metal ions have the same ground state valence electron configuration, $(n-1)d^5$, the former metal cation exhibits an impulsive mechanism, whereas the latter reacts via an insertion mechanism, apparently because of couplings with other PESs.[6,7] The tungsten system is found to have about six times larger reactivity towards dihydrogen than the molybdenum system even though W^+ has an electron configuration of $6s^15d^4$, which would be expected to react inefficiently with dihydrogen. As for Ta^+, this is a result of efficient spin–orbit coupling between surfaces of different spin. The higher reactivity for the tungsten system is also a result of the smaller endothermicity compared to the chromium and molybdenum systems,[6,7] again a result of the lanthanide contraction and relativistic effects.[16]

In contrast to the platinum system, the tantalum and tungsten systems have lower reactivity. This is partly because the latter systems have larger endothermicities. However, if energetics were the only difference, then we would expect to find similar values of σ_0, Table III. This comparison also relies on there being similar values of the parameter n, which is the case for these systems. Comparison of these values with those from the $Pt^+ + H_2(D_2)$ systems, which are about 7.5,[1] indicates that the present systems are also inhibited somewhat by other factors. We believe that this factor is likely to be the surface hopping from the high-spin to the low-spin surfaces that must occur for the tantalum and tungsten systems, which is not needed in the platinum system. The observation that the inhibition is fairly small (less than 50%) indicates that the spin–orbit interactions effectively mix PESs with different spin in the third-row metal systems.

The periodic trends in reactivity observed in this study contrast somewhat with those observed for the group 3 metal cations. There it is found that the reaction of $La^+ + H_2$ is only slightly more efficient than the reactions of Sc^+ and Y^+ (ratios of 2:1:1.5, respectively), with each exhibiting a comparable insertion mechanism.[2] The similar reactivity is partly a consequence of similar thermochemistry: $D_0(Sc^+-H) = 2.44 \pm 0.09$ eV, $D_0(Y^+-H) = 2.66 \pm 0.09$ eV, and $D_0(La^+-H) = 2.48 \pm 0.09$ eV.[2] Although lanthanum is a third-row metal, its $4f$ orbitals are empty, such that unlike Ta, W, and Pt, La is not the beneficiary of a lanthanide contraction. Consequently, its bond energy is not enhanced compared to its first and second row congeners and its reactivity is comparable.

VI. CONCLUSIONS

Ground state Ta^+ and W^+ ions are highly reactive with dihydrogen over a wide range of kinetic energies, as compared with the first-row and second-row transition metal systems. Analysis of the kinetic energy dependence of the reaction cross sections provides the BDEs of M^+-H, which are in agreement with *ab initio* calculations performed here and in the literature. These bonds are stronger than corresponding ones of the first-row and second-row transition metal systems, which is attributed to effective *sd* hybridization, a consequence of lanthanide contraction and relativistic effects.

The branching ratios observed in the $M^+ + HD$ reactions indicate that the ground state of Ta^+ and W^+ reacts with

dihydrogen largely via an insertion mechanism, with contributions from more direct mechanisms as the energy increases. This contrasts with expectations for the high-spin ground states of the metal ions that are based on diabatic reactivity "rules" established for the first-row transition metal ions. However, calculations of the potential energy surfaces indicate that the high-spin ground states of Ta^+ and W^+ interacting with H_2 are repulsive, as anticipated from these "rules." The explanation for this disparate behavior is that, unlike the first row transition metal ions, the third-row metal ions have strong spin–orbit interactions that allow extensive coupling among surfaces of differing spin. This provides low energy pathways for reactions of Ta^+ and W^+ with H_2, HD, and D_2 that involve insertion mechanisms on low-spin surfaces.

ACKNOWLEDGMENTS

This work was supported by the National Science Foundation under Grant No. CHE-9877162 and CHE-0135517. X.-G.Z. and S.-Y.S. thank Dr. Rohana Liyanage for technical help with experiments.

[1] X.-G. Zhang and P. B. Armentrout, J. Chem. Phys. **116**, 5565 (2002), preceding paper.
[2] J. L. Elkind, L. S. Sunderlin, and P. B. Armentrout, J. Phys. Chem. **93**, 3151 (1989).
[3] P. B. Armentrout, ACS Symp. Ser. **428**, 18 (1990).
[4] P. B. Armentrout, Int. Rev. Phys. Chem. **9**, 115 (1990).
[5] J. L. Elkind and P. B. Armentrout, J. Phys. Chem. **89**, 5626 (1985).
[6] J. L. Elkind and P. B. Armentrout, J. Chem. Phys. **86**, 1868 (1987).
[7] M. R. Sievers, Y.-M. Chen, and P. B. Armentrout, J. Phys. Chem. **100**, 54 (1996).
[8] S. K. Loh, D. A. Hales, L. Lian, and P. B. Armentrout, J. Chem. Phys. **90**, 5466 (1989).
[9] R. H. Schultz and P. B. Armentrout, Int. J. Mass Spectrom. Ion Processes **107**, 29 (1991).
[10] S.-Y. Shin, R. Liyanage, and P. B. Armentrout (unpublished).
[11] A. D. Becke, J. Chem. Phys. **98**, 5648 (1993).
[12] C. Lee, W. Yang, and R. G. Parr, Phys. Rev. B **37**, 785 (1988).
[13] M. J. Frisch, G. W. Trucks, H. B. Schlegel *et al.*, GAUSSIAN 98, Revision A.7, Gaussian, Inc., Pittsburgh, PA., 1998.
[14] K. P. Huber and G. Herzberg, *Molecular Spectra and Molecular Structure* (Van Nostrand Reinhold, New York, 1979), Vol. IV.
[15] P. J. Hay and W. R. Wadt, J. Chem. Phys. **82**, 299 (1985).
[16] G. Ohanessian, M. J. Brusich, and W. A. Goddard, III, J. Am. Chem. Soc. **112**, 7179 (1990).
[17] J. B. Foresman and Æ. Frisch, *Exploring Chemistry with Electronic Structure Methods*, 2nd ed. (Gaussian, Inc., Pittsburgh, 1996).
[18] C. E. Moore, *Atomic Energy Levels*, Natl. Stand. Ref. Data Ser. (U.S., Natl. Bur. Stand.) **III**, 35 (1971).
[19] X.-G. Zhang, R. Liyanage, and P. B. Armentrout, J. Am. Chem. Soc. **123**, 5563 (2001).
[20] D. G. Dai, W. Cheng, and K. Balasubramanian, J. Chem. Phys. **95**, 9094 (1991).
[21] K. Balasubramanian and Z. Ma, J. Phys. Chem. **95**, 9794 (1991).
[22] J. L. Elkind and P. B. Armentrout, J. Phys. Chem. **91**, 2037 (1987).
[23] P. B. Armentrout, in *Gas Phase Inorganic Chemistry*, edited by D. H. Russell (Plenum, New York, 1989), p. 1.
[24] P. B. Armentrout, in *Selective Hydrocarbon Activation: Principles and Progress*, edited by J. A. Davies, P. L. Watson, A. Greenberg, and J. F. Liebman (VCH, New York, 1990), p. 467.
[25] M. E. Weber, J. L. Elkind, and P. B. Armentrout, J. Chem. Phys. **84**, 1521 (1986).
[26] P. B. Armentrout, in *Advances in Gas Phase Metal Ion Chemistry*, edited by N. G. Adams and L. M. Babcock (JAI, Greenwich, 1992), Vol. 1, p. 83.
[27] H. Zhang and K. Balasubramanian, J. Phys. Chem. **96**, 6981 (1992).
[28] J. L. Elkind and P. B. Armentrout, Inorg. Chem. **25**, 1078 (1986).
[29] P. B. Armentrout and D. E. Clemmer, in *Energetics of Organometallic Species*, edited by J. A. M. Simoes and J. L. Beauchamp (Kluwer, Dordrecht, 1992), p. 321.
[30] P. B. Armentrout and B. L. Kickel, in *Organometallic Ion Chemistry*, edited by B. S. Freiser (Kluwer, Dordrecht, 1996), p. 1.
[31] Y.-M. Chen, J. L. Elkind, and P. B. Armentrout, J. Phys. Chem. **99**, 10438 (1995).
[32] L. G. M. Pettersson, C. W. Bauschlicher, Jr., S. R. Langhoff, and H. Partridge, J. Chem. Phys. **87**, 481 (1987).
[33] G. Ohanessian and W. A. Goddard, III, Acc. Chem. Res. **23**, 386 (1990).